JOURNAL OF SOLID STATE CHEMISTRY **129,** 30–36 (1997)
ARTICLE NO. SC967216

Study of the Interactions between MoO_3 and α-Fe_2O_3

Lin Dong, Kaidong Chen, and Yi Chen[1]

Chemistry Department, Nanjing University, Nanjing 210093, China

Received February 16, 1996; in revised form October 15, 1996; accepted November 4, 1996

α-Fe_3O_3-supported molybdenum catalysts were prepared by heating a mixture of MoO_3 and α-Fe_2O_3. XRD, XPS, LRS, FT–IR, and Mössbauer spectroscopy were used to study the interactions between MoO_3 and α-Fe_2O_3. At the temperature of 693 K, the dispersion capacity of MoO_3 on α-Fe_2O_3 determined by XRD and XPS is 0.80 mmol MoO_3/100 m^2 α-Fe_2O_3, i.e., 4.8 Mo^{6+}/nm^2. LRS and FT–IR results show that at low MoO_3 loading (1.8 Mo^{6+}/nm^2), Mo^{6+} cations are located in the tetrahedral sites of the α-Fe_2O_3 surface. The occcupation of octahedral surface vacant sites increases with the MoO_3 loading. Considering the fact that each Mo^{6+} is accompanied by $3O^{2-}$ anions and that α-Fe_2O_3 has a hexagonal structure, almost all the incorporated Mo^{6+} on the surface are in octahedral coordination environment. Based on the assumptions that the (001) plane of α-Fe_2O_3 is preferentially exposed on the surface and that all the usable surface vacant sites have been occupied, the formation of a close-packed layer on the α-Fe_2O_3 surface by the O^{2-} anions linked with the incorporated Mo^{6+} can be expected, which is in good agreement with the result predicted by the incorporation model proposed previously. A relationship between the residual bulk MoO_3 and the calcination time shows that Mo^{6+} ions occupy the surface vacant sites of α-Fe_2O_3 in two stages. The first stage may correspond to the migration of Mo^{6+} cations from the bulk MoO_3 to the tetrahedral surface vacant sites on the surface. The second stage may correspond to the migration of Mo^{6+} from the bulk MoO_3 into the octahedral unoccupied vacant sites. Mössbauer spectroscopy and XRD results indicate that a new phase, $Fe_2(MoO_4)_3$, is formed when the sample containing 10.0Mo^{6+}/nm^2 α-Fe_2O_3 was calcined at 743 K, suggesting that the calcination temperature is important to the interaction extent between MoO_3 and α-Fe_2O_3.

INTRODUCTION

Metal oxide–support interactions have attracted much attention because of the wide application of supported metal-oxide systems. It has been well documented that under appropriate conditions many metal oxides, such as MoO_3, WO_3, NiO, ZnO, MgO, and CdO, can be dispersed on the surfaces of supports like γ-Al_2O_3, TiO_2, ZrO_2, and zeolites, Xie and Tang (1) were the first to claim that the monolayer dispersion of many metal oxides on γ-Al_2O_3 could be realized simply by the calcination of mixtures at $\sim$723 K. Measurements of the dispersion capacity of many oxides, i.e., the maximum amount of automatically dispersed metal oxides without the existence of a bulk phase, by different experimental methods such as XRD (X-ray diffraction), XPS (X-ray photoelectron spectroscopy), and ISS (ion scattering spectroscopy) led them to explain the dispersion capacities of some metal oxides on γ-Al_2O_3. The dispersion process has been described by Knözinger as the wetting of the γ-Al_2O_3 surface by metal oxides (2). It has also been commonly accepted that interactions between γ-Al_2O_3 and the dispersed species are inevitable. In fact, it has been shown that the coordination environment of the dispersed metal cations is strongly dependent upon their loading amount as well as the calcination conditions used (3, 4). Therefore, strong impact of these factors on the properties (e.g., reducibility, magnetic properties, and catalytic activity) of γ-Al_2O_3-supported metal-oxide systems can be expected.

According to the surface structure of γ-Al_2O_3, the valence states of the supported metal oxides and the dispersion capacities of the metal oxides supported on γ-Al_2O_3, Chen and Zhang proposed a surface interaction model—"incorporation model" (5). They reported that under appropriate experimental conditions, the interaction between many metal oxides and γ-Al_2O_3 could be described by the model (5–7), assuming that the (110) plane is preferentially exposed on the surface of γ-Al_2O_3. The experimental results that support the model are the dispersion capacities of oxides containing M^+ (Li^+), M^{2+}, and M^{6+} cations and the relationship between the coordination environment of Ni^{2+} and Mo^{6+} and the loading amount of these metal oxides supported on γ-Al_2O_3. The following facts in the systems of supported metal oxides can be explained by the model.

(1) NiO, MgO, ZnO, and CdO have the same dispersion capacity, i.e., 9.0–9.8 M^{2+} ions/nm^2 γ-Al_2O_3 (5), while Li_2O has 11.4–12.0 Li^+ ions/nm^2 γ-Al_2O_3 (7).

(2) The dispersion capacities for MoO_3 and WO_3 are also the same, i.e., 4.5–5.3 M^{6+} ions/nm^2 γ-Al_2O_3 (1, 5).

(3) The dispersion capacities of NiO and MoO_3 on SiO_2 are very low (1, 5).

[1] To whom correspondence should be addressed.

0022-4596/97 $25.00

In this paper, another support, α-Fe_2O_3 with a large BET specific surface area (Hematite, 58 m^2/g), has been selected as a support to study the interaction between MoO_3 and α-Fe_2O_3 and to examine if the incorporation model can be used to discuss the dispersion capacity and the coordination environment of Mo^{6+} on the surface of the α-Fe_2O_3 support.

EXPERIMENTAL

Sample Preparation

The α-Fe_2O_3 support was calcined at 823 K for 5 h before it was used as the support to prepare MoO_3/α-Fe_2O_3 samples.

MoO_3/α-Fe_2O_3 samples were prepared by calcination of a series of mixtures of MoO_3 and α-Fe_2O_3 with different amounts of MoO_3 at 693 K in air for 24 h.

Instrumentation

XRD (X-ray diffraction) patterns were recorded using a Shimadzu XD-3A X-ray diffractometer with the Fe$K\alpha$ radiation (0.1979 nm) and a Mn filter. α-Al_2O_3 powder was used as a reference for quantitative analysis.

A V.G. Escalab MK II system was used to record XPS spectra for determining the dispersion capacity of MoO_3 supported on α-Fe_2O_3.

Laser Raman spectra (LRS) were recorded in air with a Spex Ramalog-1403 spectrometer equipped with a triple monochrometer. The 5145 Å line of a Spectra Physics Model 2000 Ar^+ laser was used for excitation. A laser power of 20 mW at the sample was applied. The spectral slit width was 300 nm, the wave-number accuracy being $\pm 2\,cm^{-1}$. To obtain the distinctive spectra, MoO_3/α-Fe_2O_3 samples have been thoroughly mixed and diluted with KBr before being pressed as disks. The same method has been used in FT–IR experiments also. All the IR spectra were taken with a Nicolet-510p FT–IR spectrometer with $\pm 2\,cm^{-1}$ resolution. Using the digital subtraction capability of the spectrometer, the support spectrum was subtracted from the sample spectra to obtain only the spectra of Mo oxide on the surface.

Mössbauer spectra were obtained with a constant-acceleration spectrometer using a 10 mCi^{57} Co/Pd source. All spectra were computer fitted with Lorentzian line shapes using a least-squares fitting procedure, and the isomer shifts (IS) are given with respect to the centroid of α-Fe at room temperature.

RESULTS AND DISCUSSION

I. Structure of α-Fe_2O_3

α-Fe_2O_3 (Hematite) is hexagonal and has the same structure as α-Al_2O_3 and α-Cr_2O_3 (8, 9). Its bulk structure can be described as a slightly distorted closest-packed array of oxygens with Fe^{3+} filling two-thirds of the octahedral sites. The (001) face is the most likely crystal plane to predominate in the external surface of these supports (8). The structure of the (001) plane is shown in Fig. 1. It can be seen that 4 vacant sites exist in a surface unit mesh of this plane, of which one-forth are octahedral sites and the others tetrahedral sites. If the radius of O^{2-} is taken as 0.14 nm, the area of a mesh is about 0.203 nm^2.

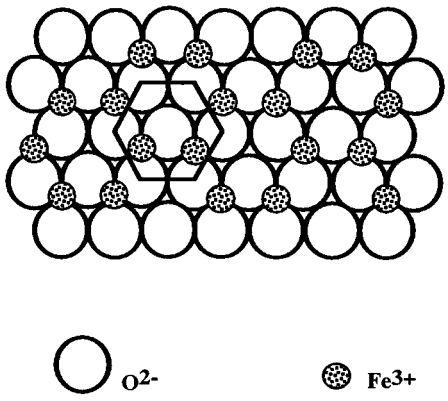

FIG. 1. Structure of the α-Fe_2O_3 (001) plane.

II. The Surface Interaction between MoO_3 and α-Fe_2O_3 at 693 K

Figure 2 shows the XRD patterns of a series of MoO_3/α-Fe_2O_3 samples with different Mo loadings before and after heat treatment at 693 K for 24 h. All the mixtures referred to in Fig. 2 (A, B, and C) show sharp peaks of crystalline MoO_3 [2θ: 29.46° (110); 32.52° (040); 34.58° (021)]. But for the low MoO_3 content samples (A and B: 1.8 and 4.2 Mo^{6+}/nm^2 α-Fe_2O_3), after being heated at 693 K, a temperature well below the melting point (1068 K) of MoO_3, the peaks of crystalline MoO_3 disappeared and the XRD patterns resemble that of the pure α-Fe_2O_3 support (D). The crystalline phase of MoO_3 has vanished but the support has remained unchanged. The experiments indicate that MoO_3 is well retained by the sample and does not escape from the sample because it did not matter whether the mixture was heated in an open or a sealed glass tube. It is also very unlikely that the crystalline phase of MoO_3 transforms into an amorphous phase upon the heat treatment. So it seems that the only reasonable answer is that MoO_3 has dispersed on the surface of the support. However, when the content of MoO_3 in the sample exceeds a critical amount (dispersion capacity), the peaks of crystalline MoO_3 do not disappear, but are markedly reduced after the heat treatment. The XRD pattern of the mixture containing 10.0 Mo^{6+}/nm^2 α-Fe_2O_3 is shown in Fig. 2C. After the mixture has been heated at 693 K for 24 h, the pattern C changes into C′, in which the

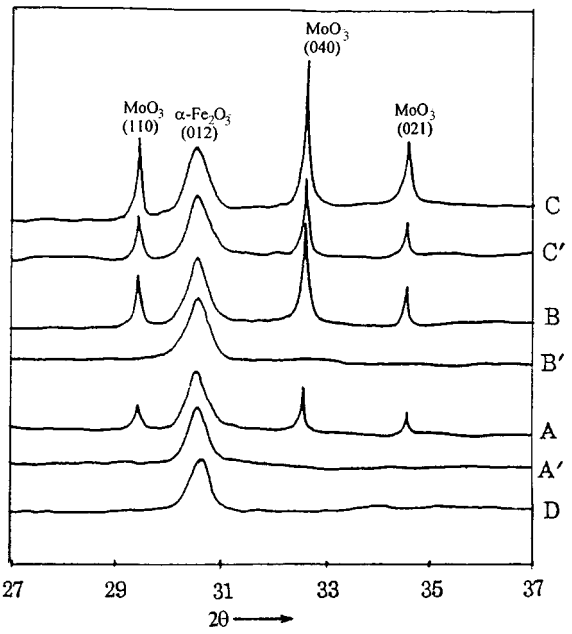

FIG. 2. XRD patterns for MoO_3/α-Fe_2O_3 samples containing different Mo loadings: A, mixture of 1.8 $Mo^{6+}/nm^2\alpha$-Fe_2O_3; A′, sample A after a heat treatment at 693 K for 24 h; B, mixture of 4.2 $Mo^{6+}/nm^2\alpha$-Fe_2O_3; B′, sample B after a heat treatment at 693 K for 24 h; C, mixture of 10.0 $Mo^{6+}/nm^2\alpha$-Fe_2O_3; C′ sample C after a heat treatment at 693 K for 24 h; D, α-Fe_2O_3 of a specific surface ($58m^2/g$).

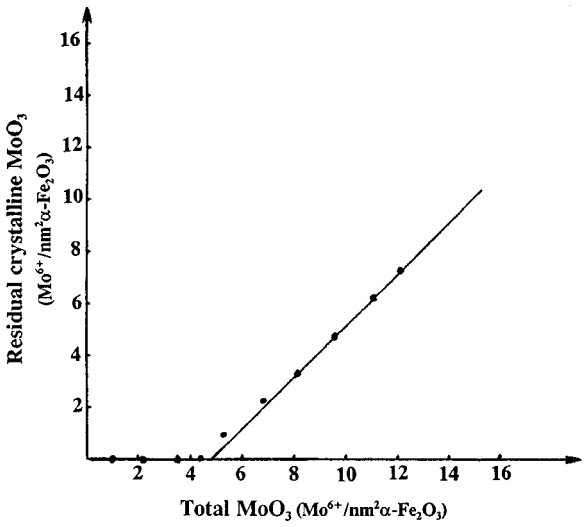

FIG. 3. Residual amount of MoO_3 versus total amount of MoO_3 in MoO_3/α-Fe_2O_3 samples after heating at 693 K for 24 h.

peaks of crystalline MoO_3 are present, but with reduced intensity, indicating that some residual crystalline MoO_3 remains. This XRD pattern does not change with increasing heating time. It suggests that heating at this temperature only causes MoO_3 to disperse onto the surface of α-Fe_2O_3 but not to diffuse into or react with the bulk α-Fe_2O_3.

Figure 3 shows the relationship of residual crystalline MoO_3 versus total amount of MoO_3 in MoO_3/α-Fe_2O_3. The amount of residual crystalline MoO_3 can be determined by XRD quantitative phase analysis (1). When the content of MoO_3 in the samples is below the dispersion capacity, no crystalline MoO_3 can be detected. But if the MoO_3 content exceeds this value, the residual MoO_3 increases with the total amount of MoO_3 as shown in Fig. 3 by the straight line. This straight line does not go through the origin but gives an intercept corresponding to the maximum dispersion capacity. In an ideal case the slope of this line is unity. The present results show that the dispersion capacity of MoO_3 supported on α-Fe_2O_3 is 4.8 Mo^{6+}/nm^2 or 0.97 Mo^{6+}/mesh.

The Mo_{3d}/Fe_{2p} XPS intensity ratio as a function of bulk Mo content for MoO_3/α-Fe_2O_3 samples is shown in Fig. 4. It increases linearly up to the Mo content of 4.8 $Mo^{6+}/nm^2\alpha$-Fe_2O_3. Obviously, the heat treatment has caused MoO_3 to disperse on the surface of α-Fe_2O_3, thus producing a stronger XPS signal. A similar phenomenon has been reported by Knözinger and Taglauer (10) and by Gui *et al.* (11). Beyond that content, a turning point appears, which corresponds to the dispersion capacity for MoO_3 on α-Fe_2O_3, (0.8 mmol $MoO_3/100m^2$ α-Fe_2O_3 or 4.8 Mo^{6+}/nm^2 α-Fe_2O_3). The Mo/Fe intensity ratio at Mo loadings exceeding 4.8 $Mo^{6+}/nm^2\alpha$-Fe_2O_3 increases more slowly than for lower loadings. This indicates that crystalline MoO_3 exists in the samples besides the surface Mo^{6+} species. This result is in good agreement with that of the XRD. However, it should be mentioned that XPS peak intensities are influenced mainly by the surface concentration and to

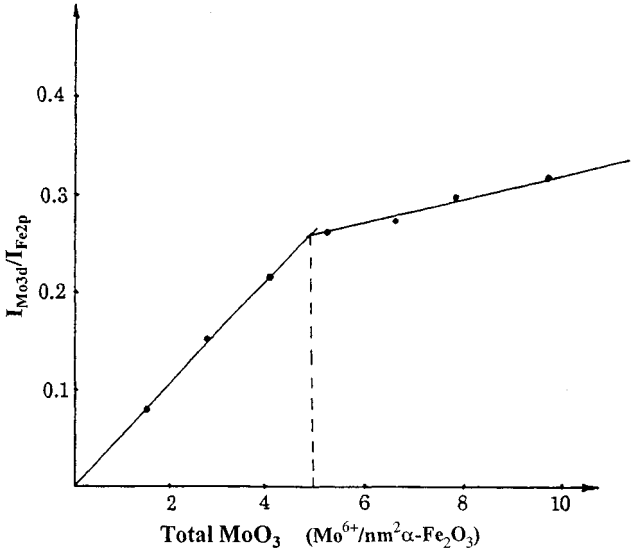

FIG. 4. XPS peak intensity ratio I_{Mo3d}/I_{Fe2p} versus the content of MoO_3 in MoO_3/α-Fe_2O_3 samples after a heat treatment at 693 K for 24 h.

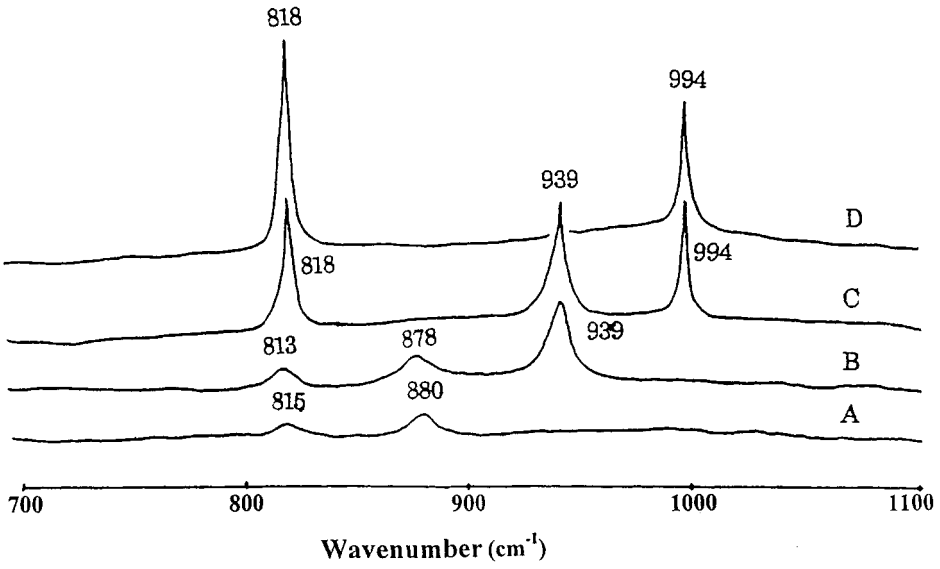

FIG. 5. Raman spectra of MoO_3/α-Fe_2O_3 (calcined at 693 K for 24 h) as a function of Mo loading (in Mo^{6+}/nm^2): A, 1.8; B, 4.1; C, 7.9; D, pure MoO_3. The intensity scale of profile C is one third of that of profiles A and B.

some extent by other factors such as physical properties of supports, especially pore-size distribution and the particle size of the metal oxide. Nevertheless, in our case, the changes in surface areas and pore-size distribution measured were insignificant, indicating that they cannot be responsible for the distinctive change in the slope of the intensity ratio versus loading line.

Figure 5 shows a representative number of LRS spectra for the samples after calcination, which provide valuable information concerning the formation of different surface species as a function of molybdenum loading. In spectra A–C, it is likely to assume that the peak 939 cm^{-1} corresponds to Mo^{6+} incorporated into octahedral surface sites, and peaks 880 and 815 cm^{-1} may correspond to the occupation of Mo^{6+} into tetrahedral surface sites (12–14). In spectrum A, the peak 939 cm^{-1} has not been observed, this can be ascribed to the predominant tetrahedral vacant sites on the surface, which may result from the more tetrahedral vacant sites on the (001) plane, i.e., Tet/Oct = 3:1. With the increases of MoO_3 from 1.8 to 4.1 Mo^{6+}/nm^2, the intensity of the 939 cm^{-1} peak is increased, indicating that there are more octahedral surface sites being occupied. It is reasonable to suggest that with increasing MoO_3 loading more Mo^{6+} species (peaks 880 and 815 cm^{-1}) are incorporated into the octahedral surface vacant sites (peak 939 cm^{-1}).

Figure 6 shows the FT–IR spectra. There are only two weak peaks at 949 and 930 cm^{-1} for the low Mo-content sample (Fig. 6A). According to the results reported by Ng (12), these two peaks may be assigned to surface Mo species. With increasing MoO_3 loading, the peak intensity of the band at 949 cm^{-1} grows and the characteristic peak (998 cm^{-1}) representing the bulk MoO_3 appears. IR spectra show that at low Mo loading (1.8 Mo^{6+}/nm^2), octahedrally coordinated Mo^{6+} surface species are formed by the incorporation of Mo^{6+} into tetrahedral and octahedral surface vacant sites. However, at high MoO_3 loadings, more of the

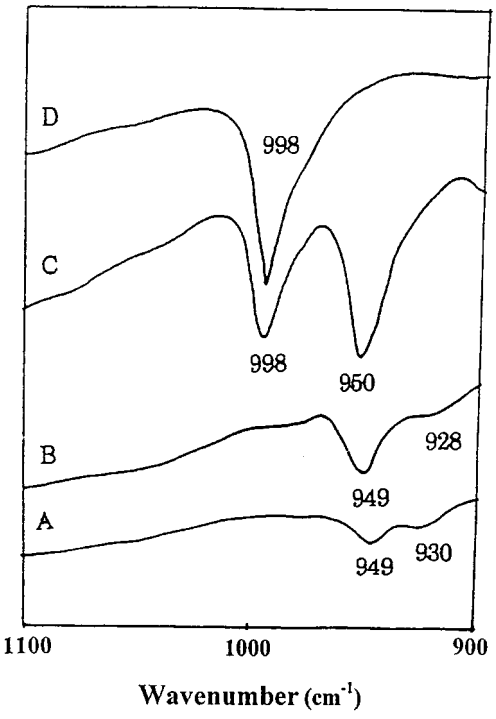

FIG. 6. Infrared spectra of calcined MoO_3/α-Fe_2O_3 (at 693 K for 24 h) as a function of loading ($Mo^{6+}/nm^2\alpha$-Fe_2O_3): A, 1.8; B, 4.1; C, 7.9; D, pure MoO_3.

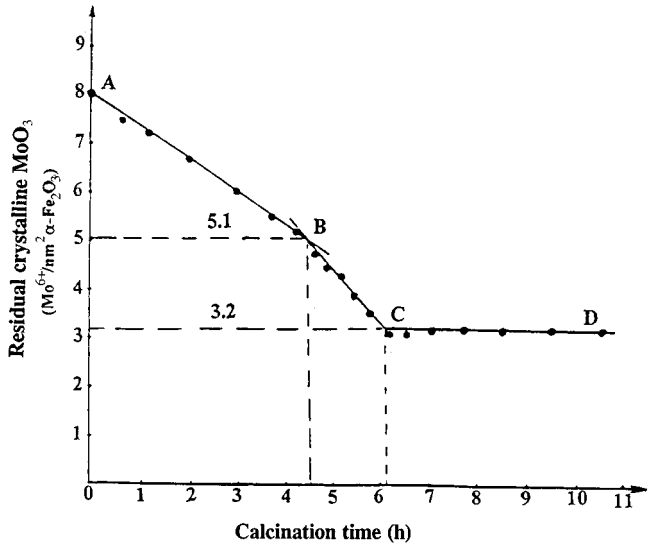

FIG. 7. The amount of dispersed MoO_3 (or residual MoO_3) in MoO_3/α-Fe_2O_3 versus calcination time at 693 K.

later species (wavenumber 949 cm^{-1}) are formed. These results are basically in agreement with those obtained by LRS.

Regarding the relationship between the dispersed MoO_3 (or residual MoO_3, determined by XRD) and the heat-treatment time, an interesting result is shown in Fig. 7, which indicates that the whole dispersion procedure at this temperature (693 K) includes three stages. In the initial stage the dispersion proceeds slowly (represented as line AB), followed by a slightly faster process (line BC), and finally the dispersed (or residual) MoO_3 amount remains unchanged. Point C corresponds to the dispersion capacity of MoO_3 on α-Fe_2O_3, which is consistent with the results obtained by the XRD and XPS quantitative analyses. It indicates that at this temperature the dispersion process completes in about 6.2 h, and which can be symbolized as:

Heat treatment less than 6.2 h

$$MoO_3(\text{bulk phase}) \rightarrow MoO_3(\text{surface species})$$

Heat treatment more than 6.2 h

$$MoO_3(\text{bulk phase}) \rightleftarrows MoO_3(\text{surface species})$$

For the different slopes of lines AB and BC, considering the results from LRS and FT–IR, it is likely that these correspond to the different stages in the formation of dispersed surface Mo^{6+} species. It is suggested that in stage AB, Mo^{6+} migrates into tetrahedral sites on the support's surface. From point B to C, Mo^{6+} from bulk MoO_3 starts migrating into the octahedral sites on the surface. These suggestions are in good agreement with the results of LRS and FT–IR. Figure 8 shows the dispersion process of MoO_3 on α-Fe_2O_3 as discussed above. It can be seen that when all the usable vacant sites are occupied, a close-packed capping O^{2-} layer is formed.

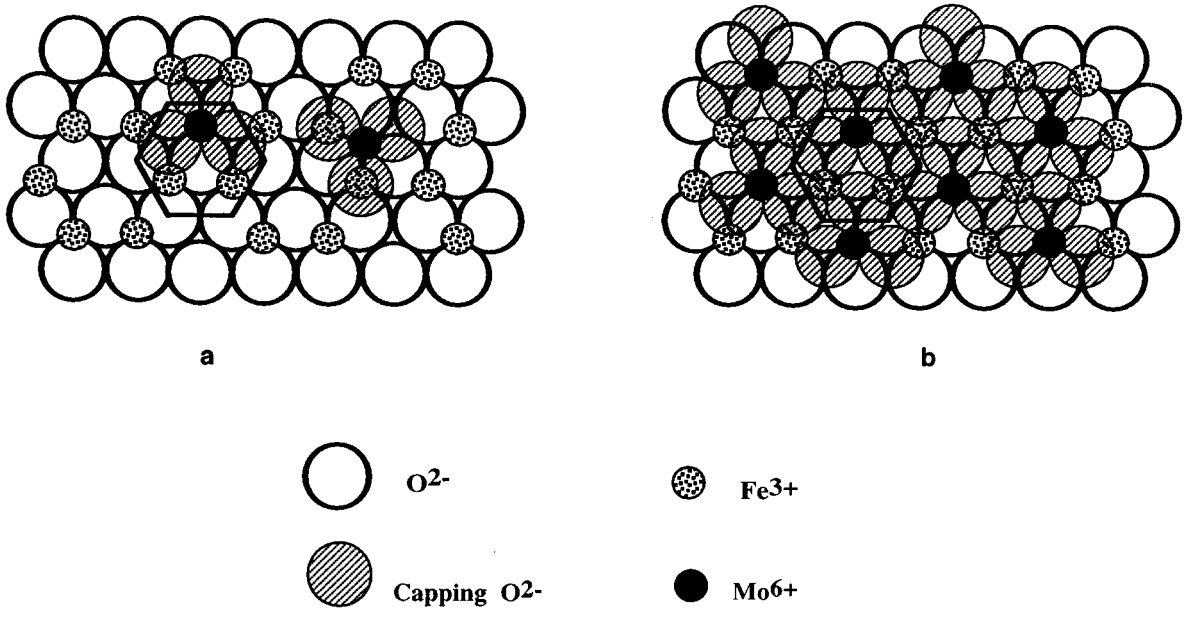

FIG. 8. A scheme for the dispersion process of MoO_3 supported on α-Fe_2O_3 at 693 K. (a) Heat treatment less than 4.5 h. (b) Heat treatment close to 6.2 h.

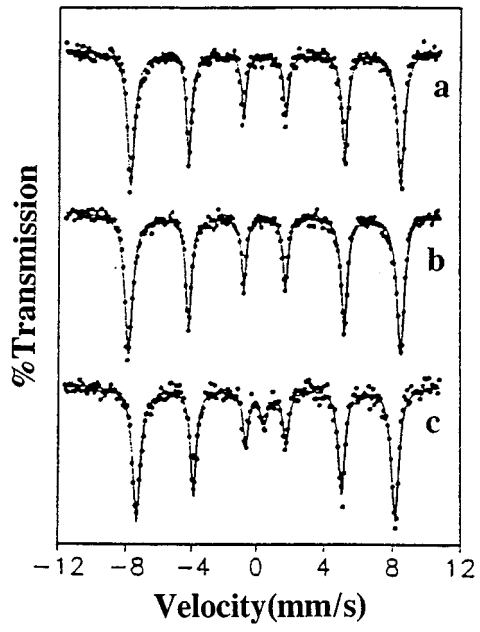

FIG. 9. Room-temperature Mössbauer spectra of a MoO_3/α-Fe_2O_3 sample containing 10.0 Mo^{6+}/nm^2 α-Fe_2O_3 calcined at different temperatures: a, pure α-Fe_2O_3; b, 693 K; c, 743 K.

III. Influence of Temperature on the Interaction Extent between MoO_3 and α-Fe_2O_3

Mössbauer spectroscopy and XRD have been used to study the effect of the temperature on the interaction between MoO_3 and α-Fe_2O_3. The Mössbauer spectra of a sample (MoO_3 content, ca. 10.0Mo^{6+}/nm^2 α-Fe_2O_3) calcined at different temperatures are shown in Fig. 9. The corresponding Mössbauer parameters are listed in Table 1. Only a sextet which is similar to that of α-Fe_2O_3 is observed for the sample calcined at 693 K. For the sample calcined at 743 K, the Mössbauer spectrum is composed of a sextet from α-Fe_2O_3 and a singlet which is assigned to $Fe_2(MoO_4)_3$ (15), indicating that a new phase $Fe_2(MoO_4)_3$ has formed. This result is consistent with that of the XRD as shown in Fig. 10. It is also pertinent to note that the hyperfine field of α-Fe_2O_3 for the sample MoO_3/α-Fe_2O_3 after treated at 743 K is only 483 KOe and much smaller than the 509 KOe of pure α-Fe_2O_3. We think that the main reason leading to this phenomenon may be the decrease of the α-Fe_2O_3 particle size due to the formation of $Fe_2(MoO_4)_3$ phase. Künding *et al.* (16) studied some properties of small α-Fe_2O_3 particles by Mössbauer spectroscopy and they confirmed that some properties of α-Fe_2O_3 changed with the particle size. For example, the hyperfine field of bulk phase α-Fe_2O_3 measured at room temperature is ca. 518 KOe. With the decrease of the particle size, the hyperfine field decreased too. For the α-Fe_2O_3 particles with diameter ca. 18 nm, the hyperfine field becomes 503 KOe. When the particle size is less than 13.5 nm, the room temperature spectrum consists only of a quadrupole-split center line corresponding to superparamagnetic α-Fe_2O_3. In our work, the average particle size of pure α-Fe_2O_3 is about 20–30 nm, hence the hyperfine field is only ca. 509 KOe and is less than the ca. 518 KOe of bulk phase α-Fe_2O_3. After the sample MoO_3/α-Fe_2O_3 is treated at 743 K, MoO_3 and some α-Fe_2O_3 form $Fe_2(MoO_4)_3$ phase, and therefore the α-Fe_2O_3 particle sizes decrease because some iron oxide is consumed in forming the $Fe_2(MoO_4)_3$ phase. This may lead to the change of the Mössbauer parameters of α-Fe_2O_3. From the above results, we can conclude that the interaction between

TABLE 1
Mössbauer Parameters of α-Fe_2O_3 and MoO_3/α-Fe_2O_3 Treated at Different Temperatures

Sample	Treatment	IS (mm/s)	QS (mm/s)	H (kOe)	Iron species
α-Fe_2O_3	823 K	0.39	− 0.17	509	α-Fe_2O_3
MoO_3/α-Fe_2O_3	693 K	0.42	− 0.12	506	α-Fe_2O_3
MoO_3/α-Fe_2O_3	743 K	0.47	− 0.18	483	α-Fe_2O_3
		0.51	0.00	0.00	$Fe_2(MoO_4)_3$

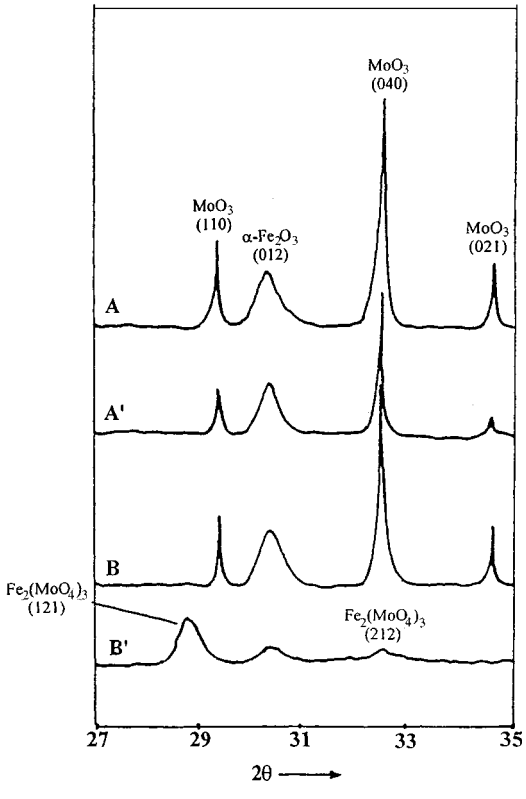

FIG. 10. XRD patterns of MoO_3/α-Fe_2O_3 sample containing 10.0Mo^{6+}/nm^2 α-Fe_2O_3 before (A, B) and after heating at 693 K (A′) and 743 K (B′), respectively.

MoO_3 and α-Fe_2O_3 is significantly affected by the calcination temperature. MoO_3 disperses on the surface of α-Fe_2O_3 at 693 K, but if the calcination temperature increases to 743 K, the solid-state reaction between MoO_3 and part of the α-Fe_2O_3 occurs and the $Fe_2(MoO_4)_3$ phase is formed.

CONCLUSIONS

(1) At 693 K, the dispersion capacity of MoO_3 supported on α-Fe_2O_3 determined by XRD and XPS is 4.8 Mo^{6+}/nm^2. With the assumption that (001) plane is preferentially exposed on the surface of α-Fe_2O_3, the capping oxygen anions linked with the incorporated Mo^{6+} form a close-packed layer, which is in agreement with the result predicted by the incorporation model.

(2) LRS and FT–IR results show that, at low Mo concentration, Mo^{6+} cations locate in tetrahedral sites of the surface of α-Fe_2O_3 support, and the occupation of the octahedral surface sites increases with the Mo loading. Taking into consideration that each incorporated Mo^{6+} is accompanied by $3O^{2-}$ anions, almost all the Mo^{6+} cations are located in octahedral sites. The relation between the calcination time and the dispersed (or residual) MoO_3 amount shows that the incorporating process of Mo^{6+} onto the surface vacancies of α-Fe_2O_3 develops in three stages. In the first stage, Mo^{6+} cations enter the tetrahedral surface vacant sites. In the second stage, Mo^{6+} cations migrate from the bulk MoO_3 phase into the surface octahedral vacancies. When the usable surface sites have been completely filled the dispersed MoO_3 amount remains unchanged and reaches a balance between the dispersion and crystallization of MoO_3.

(3) Mössbauer spectra and XRD results show that at 743 K MoO_3 reacts with α-Fe_2O_3 to form a bulk compound $Fe_2(MoO_4)_3$, indicating that the temperature significantly affects the interaction extent between MoO_3 and α-Fe_2O_3.

ACKNOWLEDGMENTS

This work was supported, in part, by the National Natural Science Foundation of China under Grant 9287010. The authors acknowledge the help of Professor Bing Zhong for supplying the α-Fe_2O_3 support with large surface area and the valuable discussions with Professors Jianyi Shen, Zheng Hu, and Yining Fan.

REFERENCES

1. Y. C. Xie and Y. Q. Tang, *Adv. Catal.* **37,** 1 (1990)
2. H. Knözinger, *in* "Proceedings, 9th International Congress on Catalysis, Calgary," Vol. 5, p. 20. Chem. Institute of Canada, Ottawa, 1988.
3. D. S. Zingg, L. E. Makovsky, R. E. Tischer, F. R. Brown, and D. M. Hercules, *J. Phys. Chem.* **84,** 2898(1980).
4. L. W. Burggraf, D. E. Leyden, R. L. Chin, and D. M. Hercules, *J. Catal.* **78,** 360 (1982).
5. Y. Chen and L. F. Zhang, *Catal. Lett.* **12,** 51 (1992).
6. Y. Chen, L. F. Zhang, J. F. Lin, and Y. S. Jin, "Catalitic Science and Technology," Vol. 1, p. 291. Kodansha, Tokyo, 1991.
7. L. F. Zhang and Y. Chen, *J. Solid State Chem.* **97,** 292 (1992).
8. H. Knözinger, *Adv. Catal.* **25,** 185 (1976).
9. M. F. Hochell, JR, C. M. Eggleston, V. B. Elings, G. A. Parks, G. E. Brown, JR, C. M. Wu, and K. Kjoller, *Am. Mineral.* **74,** 1233 (1989).
10. H. Knözinger and E. Taglauer, *in* "Catalysis," (J. J. Spivey and S. K. Agarwal, Eds.), Vol. **10**, p. 1. A specialist periodical report, The Royal Society of Chemistry, Cambridge, 1993.
11. L. Gui, Y. Liu, Q. Guo, H. Huang, and Y. Tang, *China Sci. B* **6,** 509 (1985).
12. K. Y. S. Ng and E. Gulari, *J. Catal.* **92,** 340 (1985).
13. S. R. Stampfl, Y. Chen, J. A. Dumesic, C. M. Niu, and C. G. Hill, JR, *J. Catal.* **105,** 445 (1987).
14. J. Leyrer, B. Vielhaber, M. I. Zaki, Zhuang Shuxian, J. Weitkamp, and H. Knözinger, *Mater. Chem. Phys.* **13,** 301 (1985).
15. H. L. Zhang, J. Y. Shen, and X. Ge, *J. Solid State Chem.* **117,** 127 (1995).
16. W. Kündig, H. Bömmel, G. Constabaris, and R. H. Lindquist, *Phys. Rev.* **142,** 327 (1966).